Nanocavitation in Self-Assembled Amphiphilic Block Copolymer-Modified Epoxy

Jia (Daniel) Liu,[†] Hung-Jue Sue,*[,†] Zachary J. Thompson,[‡] Frank S. Bates,[‡] Marv Dettloff,[§] George Jacob,[§] Nikhil Verghese,[§] and Ha Pham[§]

Polymer Technology Center, Department of Mechanical Engineering, Texas A&M University, College Station, Texas 77843; Department of Chemical Engineering and Materials Science, University of Minnesota, Minneapolis, Minnesota 55455; and The Dow Chemical Company, Epoxy R&D, Freeport, Texas 77541

Received May 7, 2008; Revised Manuscript Received August 7, 2008

ABSTRACT: An amphiphilic block copolymer toughener was incorporated into a liquid epoxy resin formulation and self-assembled into well-dispersed nanometer scale spherical micelles with a size of about 15 nm. The nanosized block copolymer at 5 wt % loading can significantly improve the fracture toughness of cured epoxy thermosets without reduction in modulus at room temperature and with only a slight drop in glass transition temperature. The toughening mechanisms were investigated, and it was found that the 15 nm size block copolymer micelles could cavitate to induce matrix shear banding, which mainly accounted for the observed remarkable toughening effect. Other mechanisms, such as crack tip blunting, may also play a role in the toughening. A discussion of the possible reasons responsible for the observed attractive mechanical property improvements due to the block copolymer modification is given. Implications of the present finding for designing toughened polymers are also discussed.

1. Introduction

Glassy polymers are inherently brittle if not toughened, which can greatly limit their engineering applications. Toughening of such brittle polymers via incorporation of a dispersed elastomeric phase is well-known as an effective method to improve fracture resistance and impact strength.[1−37] It has long been recognized that cavitation of the elastomeric phase is critical in promoting shear banding in various kinds of thermosets and thermoplastics.[4−8] Cavitation of rubber particles was first observed on the fracture surfaces of rubber-toughened epoxy resins more than 30 years ago.[9] Since then, many researchers have demonstrated that the major toughening mechanisms of many rubber-modified polymers are cavitation of rubber particles, followed by shear banding of the matrix.

In rubber-modified plastics, voiding can occur inside the rubber particles under hydrostatic tension. This can be manifested by a macroscopic phenomenon of stress whitening. Once the rubber particles cavitate, the hydrostatic tension near the cavitation sites is relieved, especially at the crack tip region. The stress state of the matrix near the voids is then transformed from a triaxial stress state to a biaxial stress state, which favors the initiation of shear bands.[4−8] Thus, although cavitation in itself cannot be regarded as a significant energy-absorbing process, the real role of cavitation is to relieve the triaxial stress, thereby facilitating the matrix shear banding. Quite a number of examples in the open literature support the above concept, which include the rubber toughening of epoxy,[4−19] nylon,[20−23] polycarbonate,[24−27] poly(vinyl chloride),[28−30] poly(butylene terephthalate),[31] etc.

Sultan and McGarry[10] investigated the rubber particle size effect on the fracture toughness of rubber-modified epoxies. Since then, many researchers have studied the importance of rubber particle size on toughening for a variety of polymers.[7,32−37] In the case of large particles, Pearson and Yee[7] found that particles ≥20 μm in diameter are ineffective for toughening ductile epoxy matrices. Azimi et al.[32] later indicated that lack of interaction with the crack tip process zone is the main reason for the ineffectiveness of large rubber particles for toughening. On the other hand, for small particle sizes, Bucknall and co-workers[33−35] have proposed a model based on an energy balance concept, showing that the cavitation process in the rubber particles cannot occur with particles less than 250 nm in diameter. Experimentally, some researchers have reported that 200 nm is the lower limit of rubber particle size for effective toughening.[36,37] On the contrary, the smallest rubber particle size that has been shown to cavitate is 100 nm based on core−shell rubber-modified epoxy systems.[12−19] It is noted that possible cavitation of spherical polybutadiene domains with sizes of smaller than 100 nm has also be proposed in polystyrene−polybutadiene block copolymers (BCPs).[38−40]

Recently, Bates and co-workers[41−51] discovered that amphiphilic BCPs that self-assemble into micellar structures are effective as nanodomain tougheners for epoxy resins. The BCPs usually consist of an epoxy-miscible block and an epoxy-immiscible block. In epoxy resins they can self-assemble into well-defined micro/nanostructures in the form of spherical micelles, wormlike micelles, or vesicles, depending on the molecular weight, block length, and composition of the BCPs. Addition of relatively small amount (≤5 wt %) of such BCPs has been shown to give remarkable improvement in fracture toughness. Mechanisms like debonding, cavitation, and crack deflection were proposed to account for the toughening, but no direct experimental evidence was reported.[51] Similar work on triblock copolymer toughened epoxies has also been reported recently.[52,53] However, knowledge of the toughening mechanisms responsible for such toughening effect is still lacking.

In the present study, poly(ethylene-*alt*-propylene)-*b*-poly(ethylene oxide) (PEP−PEO) diblock copolymer which self-assembles as nanoscale spherical micelles with a size of about 15 nm in diameter was chosen as a toughening agent for a commercially available epoxy resin. Mechanical properties and fracture behavior of the cured PEP−PEO-modified epoxy matrix were investigated. Conclusive evidence of *nanocavitation* of

* To whom correspondence should be addressed: Tel (979) 845-5024, Fax (979) 862-3989, e-mail hjsue@tamu.edu.
[†] Texas A&M University.
[‡] University of Minnesota.
[§] The Dow Chemical Company.

10.1021/ma801037q CCC: $40.75
Published on Web 09/24/2008

the nanosized spherical micelles is presented. The physical significance of the present finding will also be discussed.

2. Experimental Section

2.1. Materials. The epoxy monomer used for this study was diglycidyl ether of bisphenol A (DGEBA)-based epoxy resin (D.E.R. 332, Dow Chemical). The cross-linker chosen for curing the epoxy was 1,1,1-tris(4-hydroxyphenyl)ethane (THPE, Aldrich). Bisphenol-A (BPA) chain extender (PARABIS, Dow Chemical) was utilized to alter the cross-link density of the cured network in a controlled manner. Ethyltriphenylphosphonium acetate (70% in methanol, Alfa Aesar) was used as the catalyst.

The poly(ethylene-*alt*-propylene)-*b*-poly(ethylene oxide) (PEP−PEO) amphiphilic BCP was synthesized using previously described methods by Hillmyer and Bates.[54] PEO is an epoxy-miscible block, and PEP is an epoxy-immiscible block. The number-average molecular weight (M_n) of the BCP is 9100 g/mol. The weight fraction of ethylene oxide in the BCP was chosen to be 0.40.

2.2. Preparation of BCP-Modified Epoxy. The BCP and epoxy resin were mixed in a round-bottom flask and heated to 150 °C. The sample was allowed to mix until the BCP was completely dissolved into the resin. The cross-linker, THPE, was then added, and the mixture was heated up to 170 °C. Once the THPE was completely dissolved, the BPA chain extender was added and the mixture was heated up to 180 °C. When the mixture became homogeneous at 180 °C, the round-bottom flask was connected to a vacuum line for degassing. The mixture was cooled to 130 °C and remained under vacuum until no more bubbles were present. An amount of 10 μL of catalyst in an overall batch of 40 g was then added, and the mixture was stirred for 1−2 min. The sample was then poured into a mold that had been preheated to 130 °C. The mold was placed back into the oven and heated up to 200 °C for 2 h. Afterward, the cured sample was allowed to cool to room temperature in the oven.

The BCP loading in the resulting epoxy plaque was 5 wt %, and the molecular weight between cross-links (M_c) of epoxy matrix was designed to be around 1550 g/mol. The theoretical value of M_c was estimated by determining the average cross-link functionality (f_{cav}) and the average molecular weight per cross-links (M_{pc}), assuming a balanced stoichiometry:[55]

$$f_{cav} = \frac{\sum_{f=3}^{\infty} \Phi_f}{\sum_{f=3}^{\infty} \frac{\Phi_f}{f}} \tag{1}$$

where M_e is the epoxide equivalent weight of the resin, f is the

$$M_{pc} = \frac{M_e + \sum_{f=2}^{\infty} \frac{M_f}{f} \Phi_f}{\sum_{f=3}^{\infty} \frac{\Phi_f}{f}} \tag{2}$$

$$M_c = \frac{2}{f_{cav}} M_{pc} \tag{3}$$

functionality of the cross-linker/chain extender, M_f is the molecular weight of the fth functional cross-linker/chain extender, and Φ_f is the mole fraction of hydrogens provided by the fth functional cross-linker/chain extender. The cross-link density of the matrix was also experimentally estimated by measuring the equilibrium storage modulus in the rubbery state, according to Nielsen's equation.[56,57]

All the specimens were dried in a vacuum oven for at least 24 h at 80 °C prior to being characterized as described below.

2.3. Morphology Characterization. Transmission electron microscopy (TEM) was used to characterize the morphology of the BCP-toughened epoxy. The material was first microtomed at room temperature using an Ultracut E microtome and a Micro Star diamond knife. The ultrathin sections (ca. 80 nm in thickness) were collected on carbon-coated copper grids. The sections on the grids were then vapor-stained with a fresh 0.5 wt % RuO_4 aqueous solution for 10 min at ambient temperature. The stained sample sections were examined on a JEOL 1200 EX electron microscope operated at an accelerating voltage of 100 kV. TEM micrographs were taken using a calibrated Kodak electron microscope film.

2.4. Density Measurements. The density of neat epoxy and BCP-toughened epoxy samples was measured at room temperature by the displacement method in accordance with ASTM D792-91. Isopropyl alcohol, with a known density of 0.785 g/cm^3, was used for the immersion of epoxy samples. The density of epoxies was determined using the equation

$$\rho = \frac{W_a}{W_a - W_i} \rho_i \tag{4}$$

where W_a is the weight of sample in air, W_i is the weight of sample in isopropyl alcohol, and ρ_i is the density of isopropyl alcohol. Thermal mechanical analysis (TMA) was performed on a Q400 instrument (TA Instruments) to calculate the sample density above T_g.

2.5. Mechanical Property Measurements. Dynamic mechanical analysis (DMA) was performed using an RSA III instrument (TA Instruments), ranging from −120 to 150 °C at a fixed frequency of 1 Hz and a temperature increase at 5 °C per step. A sinusoidal strain amplitude of 0.05% was chosen for the analysis. The dynamic storage modulus (E') and tan δ curves were plotted as a function of temperature. The temperature at the peak in the tan δ curve was recorded as the T_g.

Room temperature tensile tests were conducted in accordance with ASTM D638-98, using an MTS servo-hydraulic test machine at a crosshead speed of 0.2 in./min (5.08 mm/min). Strain was measured by a calibrated MTS extensometer (model 632.11B-20). Young's modulus and yield stress of each sample were obtained on the basis of at least five specimens per sample. Average values and standard deviations were reported.

Fracture toughness measurements were performed on the basis of the linear elastic fracture mechanics (LEFM) approach. A single-edge-notch three-point-bending (SEN-3PB) test was used to obtain the mode I critical stress intensity (K_{IC}) of the neat epoxy and BCP-toughened epoxy in accordance with the ASTM D5045 method. The test was performed on an MTS Insight machine at a testing speed of 0.02 in./min (0.508 mm/min). Care was taken to ensure that the initial crack, generated by tapping with a fresh razor blade chilled with liquid nitrogen, exhibited a thumbnail shape crack front prior to testing. At least five specimens were used to determine K_{IC} of the samples. The critical stress intensity factor was calculated using the following equation:

$$K_{IC} = \frac{P_C S}{B W^{3/2}} f(a/W) \tag{5}$$

where P_C is the load at crack initiation, S is the span width, B is the thickness of the specimen, $f(a/W)$ is the hinge factor, W is the width of the specimen, and a is the initial crack length.

2.6. Investigation of Fracture Mechanisms. Knowledge on the sequence of fracture events is crucial in the fundamental understanding of fracture behavior of polymers. To do so, the double-notch four-point-bending (DN-4PB) test[54,58−60] was employed to probe the detailed fracture mechanisms of the BCP-toughened epoxy.

Two nearly identical cracks were cut into the same edge of a rectangular specimen beam with dimensions of 75 mm × 12.7 mm × 3.5 mm. DN-4PB tests were conducted at room temperature on an MTS Insight machine at a testing speed of 0.02 in./min (0.508 mm/min). The specimen was loaded in a four-point bending geometry with the cracks positioned on the tensile side (Figure 1a). The arrested subcritical crack tip damage zone from the core region

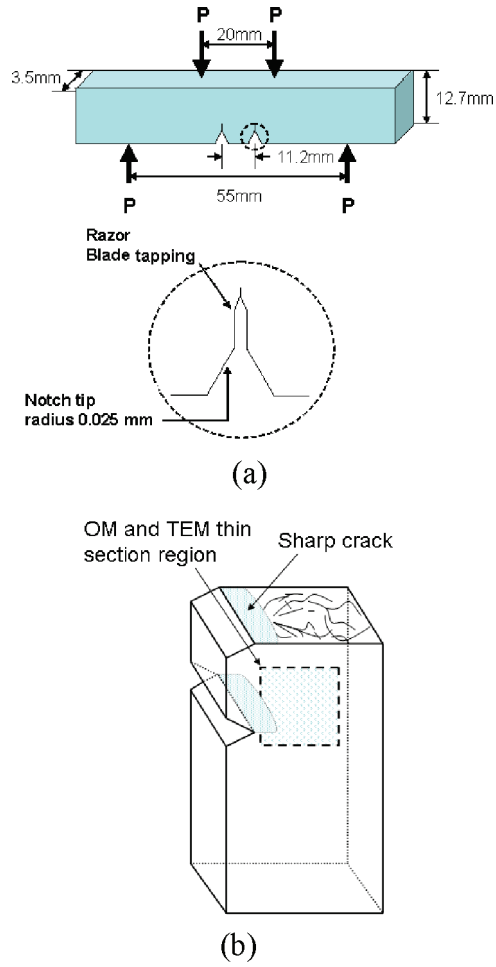

Figure 1. Schematics of (a) a DN-4PB specimen and (b) microscopy study on a DN-4PB specimen. The arrested subcritical crack tip damage zone from the core region was examined by OM and TEM.

of the specimen was isolated, trimmed, thin-sectioned, and stained for optical microscopy (OM) and TEM observations (Figure 1b).

For OM investigations, thin sections of the midsection with thickness of about 40 μm of the DN-4PB crack tip damage zone were obtained by sectioning and polishing, following the procedures described by Holik et al.[61] These thin sections were then examined using an Olympus BX60 optical microscope at both bright field and cross-polarized field modes.

To prepare TEM specimens, a block with the crack tip damage zone was diced off from the specimen and embedded in epoxy resin. After curing, the block was trimmed to about 0.3 mm × 0.3 mm, having a trapezoid shape at the tip. Then, the trimmed block was faced off by a diamond knife at room temperature, followed by microtoming and staining as aforementioned.

3. Results

3.1. Morphology of BCP-Toughened Epoxy. To the naked eye, the BCP-toughened epoxy appears transparent without aggregations, similar to neat epoxy. The TEM micrographs of the RuO_4-stained sample are shown in Figures 2a,b. The BCP phase was stained by the heavy metal and appears dark in the images while the light surroundings are epoxy matrix. The TEM micrographs show that the BCP has been self-assembled into well-defined spherical micelles and is homogeneously dispersed in the epoxy matrix. No aggregation or macrophase separation was found, and the diameter of the PEP-rich core is around 15 nm, which is found consistent with the relationship between the molecular weight and the size of BCPs.[45] An illustrative cartoon of the nanostructured morphology is presented in Figure 2c.

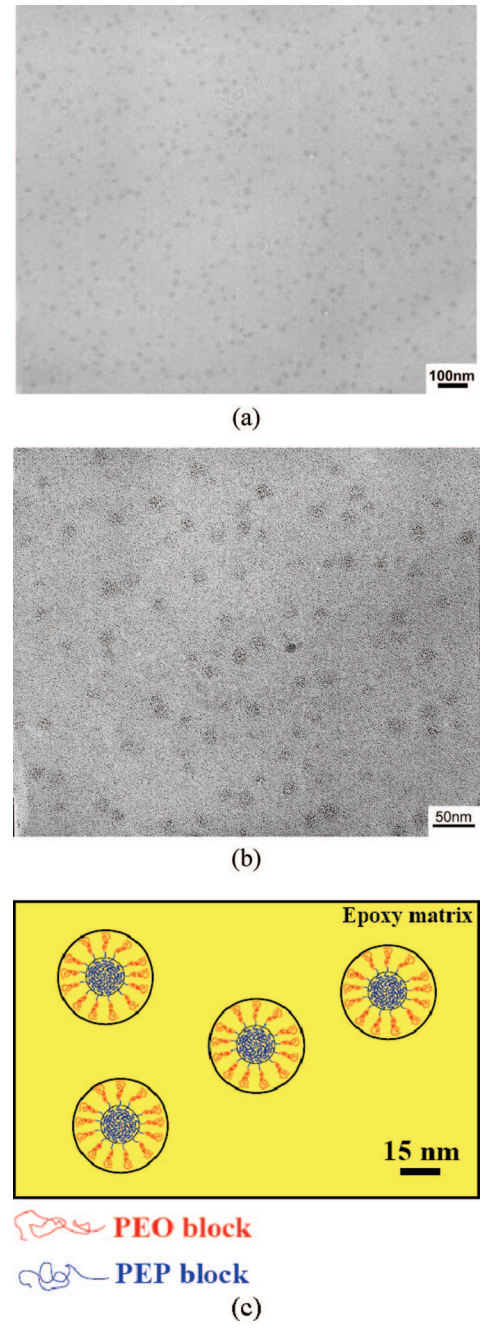

Figure 2. Nanostructured morphology of BCP-toughened epoxy: TEM micrographs at (a) low magnification and (b) high magnification and a schematic illustration (c). The amphiphilic diblock copolymer consists of an epoxy-miscible PEO block and an epoxy-immiscible PEP block and forms as spherical micelles with an average diameter of 15 nm. The BCP phase was stained by RuO_4 prior to the TEM observation and shows a darker color in the micrographs.

3.2. Dynamic Mechanical Behavior. The DMA plots are presented in Figure 3, and the storage modulus and T_g values are summarized in Table 1. A slight T_g drop of about 5 °C is observed for the BCP-toughened epoxy sample. Relative to the neat epoxy, adding BCP phase shows a slight increase in storage modulus below room temperature and a drop at the rubbery plateau region. Interestingly, the BCP-toughened epoxy exhibits a broader T_g peak and higher tan δ values at temperatures between 0 °C and the α-relaxation peak (T_g). This suggests the participation of the BCP in epoxy network formation and increased damping characteristics of the BCP-toughened epoxy. This finding signifies that the addition of the BCP enhances the energy dissipation capacity of the epoxy matrix above 0

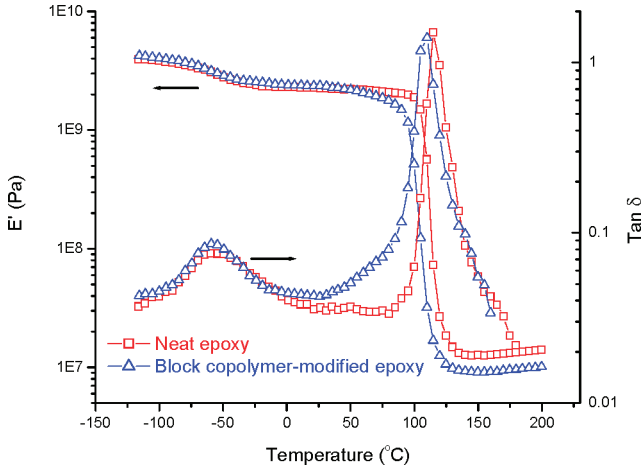

Figure 3. DMA plots of neat epoxy and BCP-toughened epoxy. Storage modulus (E') and tan δ curves are presented. The temperature maximum peak in the tan δ curve is recorded as glass transition temperature (T_g). The storage modulus and T_g values are summarized in Table 1.

Table 1. Storage Modulus, T_g, and Fracture Toughness Values of Neat Epoxy and BCP-Toughened Epoxy

	neat epoxy $T_g = 115$ °C	BCP-toughened epoxy $T_g = 110$ °C
storage modulus (Pa)		
at low temp (−100 °C)	3.86×10^9	4.04×10^9
at room temp (25 °C)	2.25×10^9	2.36×10^9
at rubbery plateau	1.41×10^7	1.01×10^7
fracture toughness, K_{IC} (MPa m$^{1/2}$)	0.96 ± 0.04	2.73 ± 0.08

°C. This finding also implies that the mechanical properties of BCP-toughened epoxy can become quite rate-sensitive. The rate sensitivity issue of BCP-toughened epoxy will be addressed in a separate paper.[62]

Additionally, the shear equilibrium storage modulus in the rubbery state (G_r) was used to determine the cross-link density of the epoxy. According to Nielsen's semiempirical equation,[56,57] the molecular weight between cross-links (M_c) can be estimated by the following equation:

$$\log G_r = 6.0 + \frac{293\rho}{M_c} \tag{6}$$

where ρ is the density of the polymer in g/cm^3, G_r in Pa, and M_c in g/mol. Since the density of the neat epoxy plaque at room temperature was measured by the displacement method as 1.20 g/cm^3, the density in the rubbery state was calculated to be 1.11 g/cm^3 (ρ), based on the coefficient of thermal expansion (CTE) information obtained from TMA. The G_r value is assumed to be related to the flexural equilibrium storage modulus, E_r, in the following manner:

$$E_r = 2G_r(1 + \upsilon) \tag{7}$$

with υ being the Poisson's ratio and assumed to be 0.5, which is typical for a rubbery material. E_r obtained from the DMA measurements is 1.41×10^7 Pa, which gives an estimated M_c of about 480 g/mol. It is noted that there is a significant discrepancy between the experimentally measured M_c via Nielsen's equation and the expected theoretical value.

3.3. Tensile Behavior. The engineering stress−true strain curves of neat epoxy and BCP-toughened epoxy are plotted in Figure 4. The Young's moduli and yield stresses are summarized in Table 2. It is clearly shown that addition of BCP toughener has no reduction in Young's modulus at room temperature, which is consistent with the results obtained from DMA. Meanwhile, the presence of BCP has resulted in pronounced

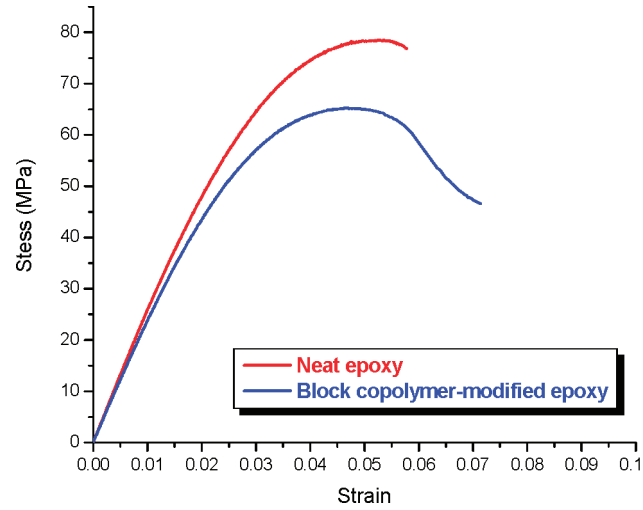

Figure 4. Engineering stress−strain curves of neat epoxy and BCP-toughened epoxy. The Young's modulus and yield stress values are summarized in Table 2.

Table 2. Young's Modulus and Yield Stress Values of Neat Epoxy and BCP-Toughened Epoxy

	neat epoxy	BCP-toughened epoxy
Young's modulus (GPa)	2.59 ± 0.06	2.58 ± 0.05
yield stress (MPa)	77.7 ± 1.1	65.8 ± 0.4

shear yielding of the epoxy matrix, with a lower yield stress. The increase in ductility and a drop of yield stress may facilitate the formation of crack tip blunting, which will be discussed below.

3.4. Fracture Toughness Measurements. The K_{IC} values of neat epoxy and BCP-toughened epoxy are summarized in Table 1. A significant improvement in K_{IC} (by 180%) over neat epoxy is observed. To show evidence of stress whitening, the fracture surfaces of the samples were recorded via a digital camera and are shown in Figure 5. In contrast to the neat epoxy, the BCP-toughened epoxy clearly shows a stress-whitening zone in front of the initial crack line. This stress-whitening phenomenon is indicative of the existence of some form of cavitation in the crack tip region. Cavitation can be due to debonding or internal cavitation of the BCP micelles or both. Although unlikely, the cavitation can also be due to the presence of microcracking or crazing. To unambiguously determine the source(s) for the observed stress-whitening zone, OM and TEM observations were conducted and are described below.

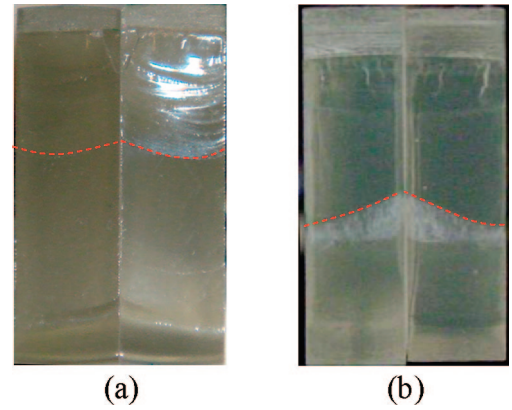

Figure 5. Fracture surfaces of (a) neat epoxy and (b) BCP-toughened epoxy after SEN-3PB tests. A stress-whitening zone was clearly observed in front of the initial crack, as seen in (b). The red dashed lines represent the initial crack marks.

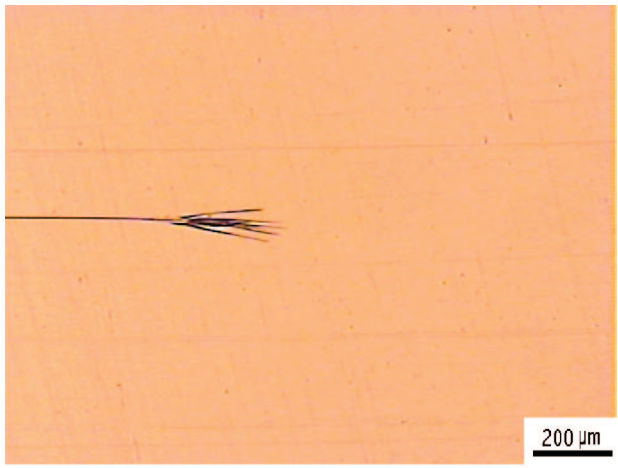

(a)

(b)

Figure 6. OM images of the BCP-toughened epoxy DN-4PB specimen with the subcritical crack tip damage zone at (a) bright field and (b) cross-polarized light field. The crack propagates from left to right. The images were taken at the same location.

3.5. Toughening Mechanisms Studies. The toughening mechanisms of the BCP-toughened epoxy were investigated via the observation of the survived crack tip damage zone of the DN-4PB specimens using OM and TEM.

Microcrack-like damage in BCP-toughened epoxy can be observed by OM under bright field in the crack tip region (Figure 6a). This microcrack-like damage feature can be formed due to the presence of dilatation bands,[12,13,16,18,63] microcracks, or crazes. Meanwhile, a small birefringent zone is observed under the cross-polarized light (Figure 6b), indicating a shear banding process. Considering the significant improvement in fracture toughness, the size of the shear banding zone seems too small to account for this improvement. Thus, we surmise that other toughening mechanisms, such as crack tip blunting,[64] may also play a role in the toughening process. This fact can be corroborated by the lower yield stress of the BCP-toughened epoxy (see Figure 4 and Table 2). A reduction of yield stress implies that it is easier to undergo plastic deformation ahead of the crack tip. A larger scale plastic deformation will lead to crack tip blunting, thereby increasing the fracture toughness of the polymer. An estimate of fracture toughness improvement due to crack tip blunting is calculated following the work of Kinloch and Williams.[64] This results in an increase of 20% in fracture toughness, which is only a small portion of the total fracture toughness increase (180%). The majority of the toughening effect therefore appears to be coming from the rubber particle cavitation-induced shear banding of the matrix.

It should be noted that OM does not have sufficient resolution to show a BCP cavitation zone as in other rubber-toughened epoxy systems where the rubber particle sizes are greater than 100 nm. TEM observation is needed to conclusively identify this toughening mechanism.

The damage zone of the DN-4PB specimen was examined using TEM. In the region adjacent to the crack wake (Figure 7a), cavitation is clearly shown inside the elongated and orientated BCP micelles. In the region slightly above (Figure 7b), the elongation and orientation of the micelles are greatly reduced, but the cavitation of the BCP micelles is still observed. In contrast, in the region outside the damage zone (Figure 7c), neither shape change nor cavitation of the BCP micelles is observed. This has morphology similar to the uncracked specimen shown in Figure 2. TEM micrographs in Figures 7a,b clearly show that cavitation of the BCP micelles are present around the crack tip and crack wake. Detailed observation suggests that the cavitation takes place inside the BCP phase, not at the micelle−epoxy interface. This cavitation phenomenon is consistent with the stress-whitening feature shown in Figure 5b. Since the BCP micelles show significant shape changes, this suggests that the epoxy around the BCP micelles have undergone equally significant amount of shear deformation. As a result, a cavitation-induced matrix shear banding process is believed to be at least partially accounted for the effective toughening of BCP-toughened epoxy. It is important to mention that the *nanocavitation* phenomenon observed in the 15 nm BCP particles is the smallest rubber particle size experimentally shown to cavitate and to promote shear banding of a polymer matrix. The sequence of events in the cavitation-induced shear banding mechanism is schematically illustrated in Figure 8. It is also worth mentioning that, unlike other studies,[12,13,16,18,63] dilatation bands around the crack tip region found in OM were not observed by TEM even after exhaustive attempts. This may be due to the scarce or fragmented formation of dilatation bands in the crack tip region.

4. Discussion

4.1. Criterion for Rubber Particle Cavitation. In 1993, Lazzeri and Bucknall[33] established a cavitation model for rubber toughening based on energy balance calculations. The assumptions for their models are summarized as follows:

(I) The largest defects within a typical rubber particle under triaxial tension are nanovoids with dimensions of the order of a few nanometers.

(II) These nanovoids will expand only if the resulting release of stored volumetric strain energy is sufficient both to increase the surface area of the void and to stretch the surrounding layers of rubber.

Assuming that the void is a sphere of radius r located at the center of a spherical rubber particle of radius R, which is well bonded to the polymer matrix, the strain energy of the rubber particle immediately before the initiation of cavitation is given by

$$U_0 = \frac{4}{3}\pi R^3 W^* = \frac{2}{3}\pi R^3 K \Delta_{V0}^{\ 2} \tag{8}$$

where W^* is the stored energy density of rubber, K is bulk modulus of rubber, and Δ_{V0} is volume strain within the rubber phase immediately before cavitation.

The volume fraction of the cavity is r^3/R^3, and thus the resulting volume strain within the cavitated rubber particle is $\Delta_{V0} - r^3/R^3$.

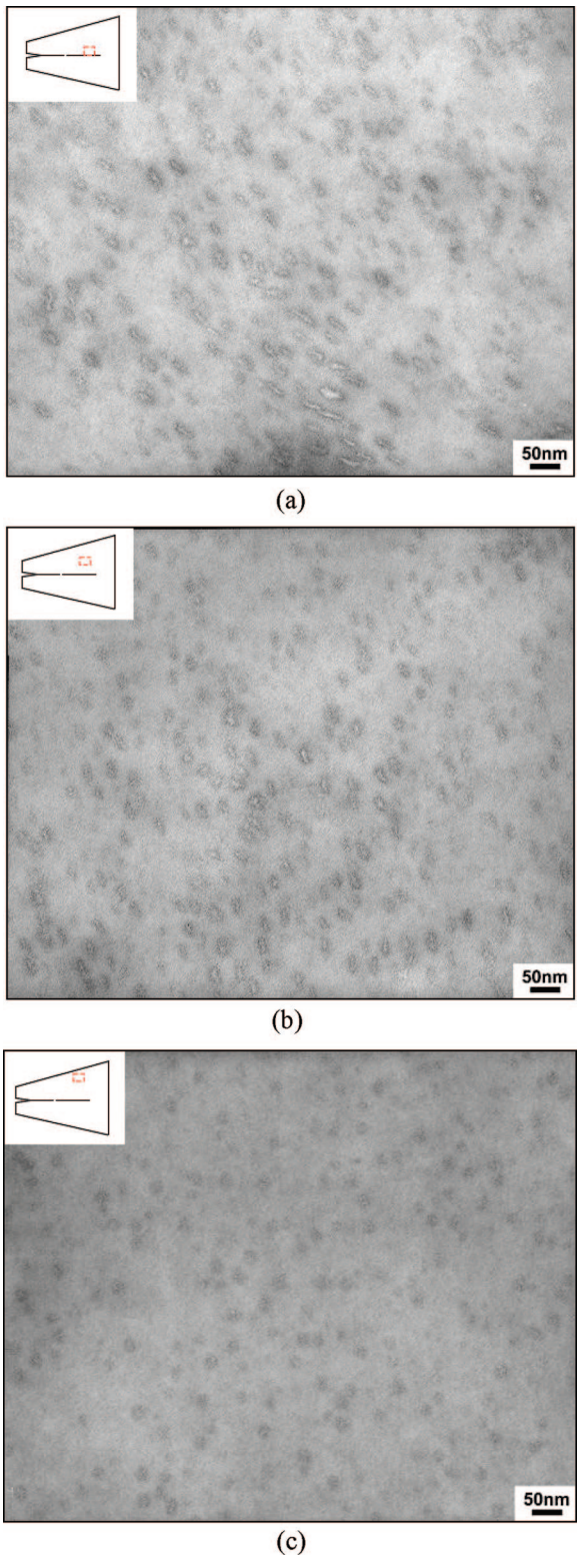

Figure 7. TEM micrographs of the BCP-toughened epoxy DN-4PB specimen at different locations: (a) adjacent to the crack wake, (b) some distance (in a range of 0.8−1.6 μm) from the crack wake, and (c) further away (more than 1.6 μm) from the crack wake. Insets demonstrate the spots where TEM micrographs were taken for each case. The BCP phase was stained by RuO_4 prior to the TEM observation.

The process of cavitation introduces two additional contributions to the total energy of the rubber particle: (i) a surface energy $4\pi r^2\Gamma$, where Γ is the surface tension of rubber phase, and (ii) a shear strain energy of $\int W_S^* \, dV$ required to stretch the surrounding rubber

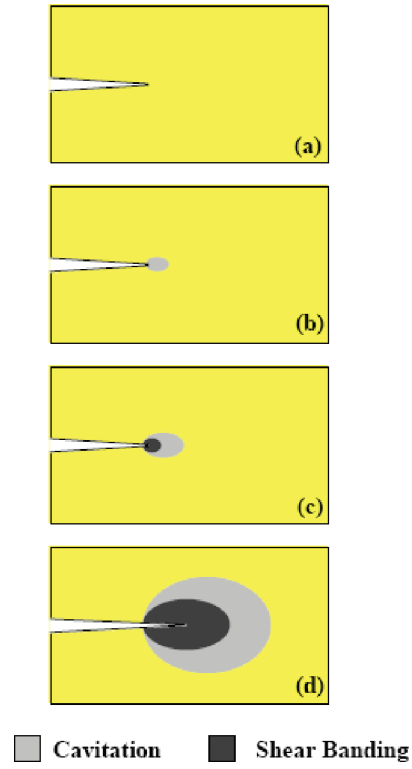

Figure 8. An illustration of the sequence of cavitation-induced shear banding process as one of the toughening mechanisms in BCP-toughened epoxy: (a) initiation of a starting crack; (b) formation of a BCP cavitation zone at the crack tip when the specimen is loaded; (c) expansion of the cavitation zone and initiation of a matrix shear banding zone at the crack tip when the hydrostatic stress is relieved by the cavitation; (d) crack propagates when the shear strain energy builds up to a critical value, with a damage zone surrounding the crack. The sizes of the crack, cavitation, and shear banding zone are not drawn to scale.

to allow the cavity to expand. Therefore, the total energy of a rubber particle after cavitation is given by

$$U = \frac{2}{3}\pi R^3 K\left(\Delta_{V0} - \frac{r^3}{R^3}\right)^2 + 4\pi r^2\Gamma + \int W_S^* \, dV \qquad (9)$$

After a series of mathematical derivation and transformation, the final expression of the energy of a cavitated particle is then where G is shear modulus of rubber, ρ is density ratio of rubber

$$U = \frac{2}{3}\pi K R^3\left[\left(\Delta_{V0} - \frac{r^3}{R^3}\right)^2 + \frac{6\Gamma}{KR}\frac{r^2}{R^2} + \frac{3G\rho F(\lambda_f)}{K}\frac{r^3}{R^3}\right] \qquad (10)$$

before and after cavitation, and λ_f is the extension ratio of the rubber at failure in equibiaxial tension.[33]

As mentioned before, the criterion for rubber particle cavitation is that the energy released during cavitation has to be greater than the total energy required to form a cavity. Lazzeri and Bucknall plotted eq 10 in terms of the reduced variables U/U_0 and r/R, where U_0 is the energy of a rubber particle immediately before cavitation (eq 8), by keeping Δ_{V0} constant at 0.004 and varying R from 0.1 to 100 μm (Figure 9a). The calculation for the plots is based on a rubber with shear modulus $G = 0.4$ MPa, bulk modulus $K = 2$ GPa, surface tension $\Gamma = 0.03$ N m^{-1}, $\rho = 1.0$, and $F(\lambda_f) = 1.0$. On the basis of the plots, the authors found that only rubber particles with radii larger than 125 nm are able to cavitate under these conditions.

Modifications of this energy balance model and a few other models have been proposed, yet without much difference in the prediction of particle size effect.[34,35,65,66] Furthermore, a recent finite element analysis effort also confirms the ineffectiveness

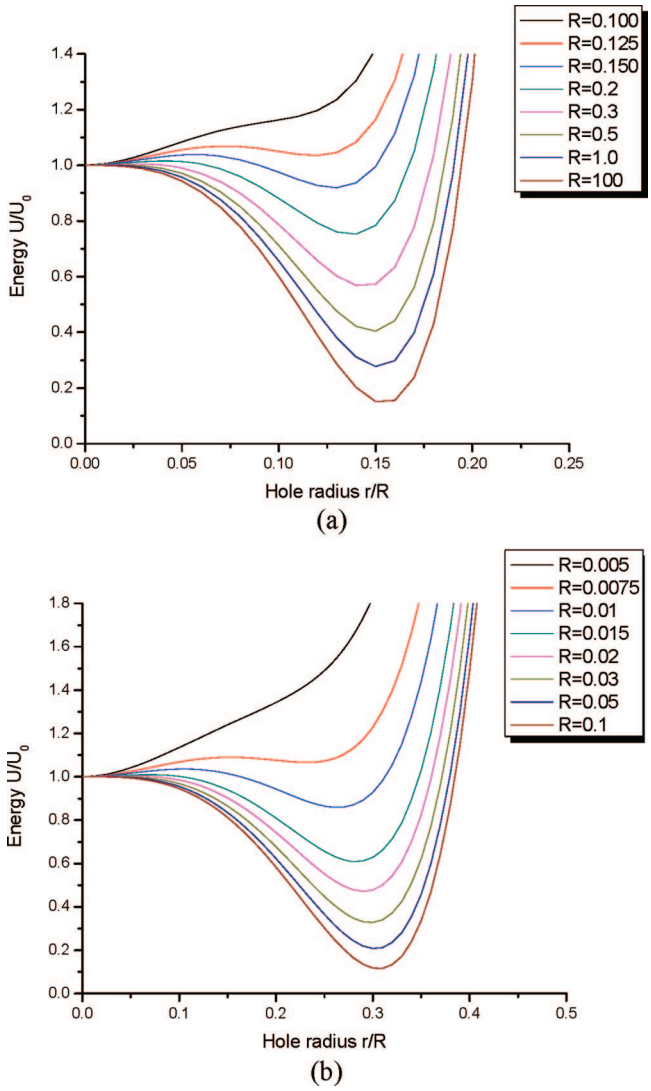

Figure 9. Calculated potential energy of a cavitated rubber particle as a function of the reduced radius of cavity, r/R, based on Lazzeri and Bucknall's energy balance model, at rubber particle volume strains of Δ_{V0} = (a) 0.004 and (b) 0.03. The curves were generated using eq 10 with various particle radii R (in μm) and G = 0.4 MPa, K = 2000 MPa, Γ = 0.03 N m^{-1}, ρ = 1.0, and $F(\lambda_f)$ = 1.0.

of small toughening particles for initiating shear banding formation.[67] Some experimental studies have supported the lower size limit of rubber particle cavitation to be about 0.2 μm, as proposed by various models.[36,37] However, cavitation of rubber particles having 100 nm in size has been repeatedly observed in the toughening of various kinds of thermosetting matrices.[12−19] In this study, clear evidence of nanocavitation of BCP micelle particles in epoxy is shown, and the size of the particles is definitely much smaller than the sizes predicted by the energy balance model under the prescribed conditions.

4.2. Nanocavitation Phenomenon in BCP-Toughened Epoxy. It is important to note that, for a given volume strain the rubber particles experience, there exists a minimal rubber particle size for cavitation. Such a correlation was illustrated by Bucknall.[68] The $U/U_0 \sim r/R$ plots with a larger volume strain of Δ_{V0} = 0.03 are illustrated in Figure 9b. Under this condition, the lower limit of particle diameter for cavitation is downshifted to 15 nm. This suggests that, on the basis of the above theory, a volume strain of at least 0.03 is experienced by the BCP for cavitation to occur. Experimental observation of the residual volume strain around the cavitated BCP based on the size change

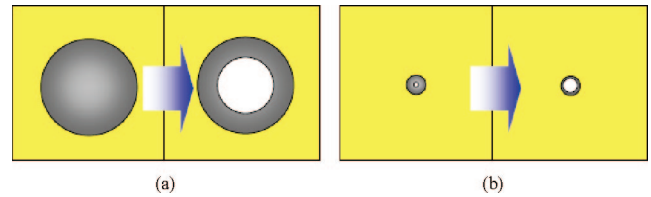

Figure 10. Schematic illustration of the cavitation processes based on (a) Lazzeri and Bucknall's model[33] and (b) the present work. Lazzeri and Bucknall neglected the energy contribution from the pre-existence of transient nanovoids within rubber particles, while that part has to be considered when dealing with nanometer-sized particles.

of the particles shown in Figure 7 is found to be greater than 0.03. Thus, it is possible that the high volume strain the epoxy matrix and BCP experience induces the 15 nm BCP particles to cavitate. However, the question as to why experimental observations made by others did not show optimal toughening effect for sizes below 0.2 μm[36,37,67] remains unanswered.

Another consideration in explaining nanocavitation is the pre-existence of transient voids in BCP. The model proposed by Lazzeri and Bucknall assumes pre-existence of nanovoids with dimensions on the order of a few nanometers in rubber particles and the cavitation is a process of nanovoid expansion. However, their criteria were based on the energy conservation between the initial state (noncavitated rubber particles) and the final state (cavitated rubber particles) without consideration of the true onset of the cavitation event. This is because of the difficulty associated with calculation of the energy or stress states at such a small scale, either from a molecular point of view or from a mechanics point of view. The consideration at such a small scale does not need to be included when applying Lazzeri and Bucknall's model in large rubber particle size cases ($\geq$100 nm). In smaller rubber particle cases, however, the model may need refinement.

The pre-existing cavities are believed to be the transient nanovoids in the rubber phase, in the form of free volume, with the size ranging from a few angstroms to a few nanometers.[69−72] The size of the pre-existing voids is similar to the size of the BCP (around 15 nm) utilized in the present study. Therefore, to construct an energy balance criterion for the system with such small rubber domains, the contribution from the pre-existence of nanovoids has to be taken into account for the energy calculation. In other words, the difference between the case Lazzeri and Bucknall[33] based their model on and the cavitation phenomenon observed in this study may lie in the consideration of the cavitation initiation from the pre-existing "holes". An illustrative comparison of the two different scenarios is shown in Figure 10.

Another important factor that should be considered is the distinction between the void expansion process in an ideal rubber particle and in a BCP micelle particle. An ideal rubber can be regarded as randomly coiled long flexible molecules with physical entanglements and/or chemical cross-links (if vulcanized).[73,74] The stretching of a rubber particle involves either the stretching of polymer network or disentanglement of molecules, or both. In the case of an ideal rubber, only the stretching of the polymer network is present and can be considered as elastic deformation, which stores potential energy in the system. In order to make cavitation of an ideal rubber a thermodynamically favorable process, breakage of covalent bonds will eventually occur, which requires a large amount of energy. On the other hand, in the case of self-assembled BCP, the molecules are generally well organized into micelle structure (see the schematic structure in Figure 2c). Thus, the expansion of micelle particles is simply a separation of adjacent molecules, which only involves destruction of secondary bonds like van

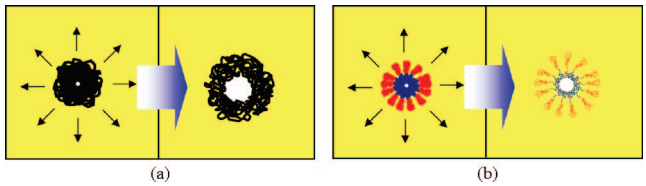

Figure 11. Schematic illustration of the two different expansion processes in (a) an ideal rubber particle and (b) a BCP micelle particle. The size expansion of the voids and the particles are not drawn to scale.

der Waals forces or hydrogen bonds. Besides, the more the expansion of the micelle particles, the weaker the attraction between the molecules becomes, making cavitation more favorable. Comparing the above two scenarios, it is easy to understand that the strain energy required for cavitation in a BCP micelle particle should be much less than that for an ideal rubber particle case. For clarity, the difference between the two expansion scenarios is sketched in Figure 11.

The actual cavitation process in such a small scale is likely to be far more complicated. In-depth efforts are still needed for physical understanding of the nanocavitation phenomenon. The matrix is also believed to play an important role in the cavitation process and its resulting toughening effect. This fact is indicated by the significant differences in their DMA tan δ curves (Figure 3) and a strong strain rate dependency of fracture toughness of this BCP-toughened epoxy system.[62] This issue will be discussed in a subsequent paper.

4.3. Other Toughening Mechanisms. Although it is evident that BCP cavitation and epoxy matrix shear banding are the two important mechanisms responsible for the observed toughening effect, crack tip blunting and the formation of dilatation bands around the crack tip region may also contribute to the toughening. It appears that rubber cavitation and shear banding of the matrix are the main causes for the observed significant improvement in fracture toughness. The contribution from crack tip blunting and the scarce dilatation bands found in OM will contribute to the toughening but to a lesser degree.

4.4. Implication of the Present Findings. The present and previous findings[18] suggest that it is feasible to simultaneously increase fracture toughness while maintaining the Young's modulus and T_g of epoxies. Generally speaking, T_g appears to be affected by larger scale main-chain motions, such as molecular motions involving the scales of distance between cross-links and multimonomer length scale.[18,75,76] Ductility and toughenability involve smaller scale cooperative molecular motions, which can still be several monomer units long.[75,76] The increase in *intra*chain cooperative motions will favor the formation of dynamic "free volumes", which facilitates the material to relax the imposed stresses. In the case of modulus, it seems to be influenced more by backbone rigidity, chain rotation, and localized small-scale molecular motions. Some researchers have also correlated the macroscopic mechanical properties to the *inter*chain packing.[77] The size scale that will influence the above properties strongly depends on the type of polymer matrices involved. Also, the sub-T_g or higher-order transitions are considered to be related to mechanical properties and fracture behaviors.[76,78]

It should be noted that the holes present due to density fluctuation inside a polymer matrix are in a range of 2.5−5.0 Å in size, as measured by small-angle X-ray scattering[79,80] and positron annihilation lifetime spectroscopy.[80,81] Meanwhile, the typical radius of gyration of a polymer chain is around 30 nm. In the case of networked epoxy systems, the increase in the rigidity of epoxy monomers will normally result in larger holes because rigid polymer chains are more difficult to achieve a dense packing than the flexible ones. Variations in cross-link density, however, have not been found to lead to a systematic change in the hole sizes, although they should influence the chain packing.[81]

The above literature findings strongly suggest that the molecular size scales that will influence the modulus, ductility, and T_g properties range from a few angstroms to tens of nanometers. The domain size of the PEP-rich phase for the present study is about 15 nm. Assuming that the BCP forms a morphology with a PEP core and PEO tails extending freely into epoxy matrix, the PEO−epoxy intermixing phase that resides at the interphase between neat epoxy and PEP-rich phase is at least 7−8 nm. The corresponding effective volume fraction of BCP, including PEP core and PEO−epoxy interphase, is estimated to be at least 0.30.[45] If considering the average surface-to-surface interparticle distance (i.e., matrix ligament thickness) is around 30 nm based on TEM image analysis, the PEO−epoxy interphase where epoxy and PEO intermix is expected to have a great influence on the matrix physical and mechanical properties.

According to the DMA finding shown in Figure 3, the PEO−epoxy interphase has greatly altered the dynamic mechanical characteristics of the epoxy matrix. The presence of the PEO−epoxy molecular intermixing layer appears to be able to shield epoxy from lowering its modulus due to the presence of PEP-rich rubber phase at room temperature. However, as the temperature rises above 50 °C, the modulus of the BCP-toughened epoxy will drop significantly below that of the neat epoxy matrix. The tan δ values increase sharply as temperature rises above room temperature, which implies that the rate sensitivity on the mechanical properties of BCP-toughened epoxy is likely to be high. The above evidence strongly suggests that the epoxy network and its molecular motions are greatly altered by the presence of PEO-rich phase in epoxy. Consequently, the modulus, T_g, ductility, and fracture toughness of epoxy are all altered, irrespective of the presence of the PEP-rich phase. It should be noted that it is unclear if continuum mechanics still applies for the BCP-toughened epoxy system at the 15 nm length scale. If not, totally different interpretation on the present findings may be warranted.

Although this research focuses on polymer toughening at nanoscale, many other factors, such as cross-link density, monomer rigidity, concentration of toughener phase, size, and geometry of toughening agent, still need to be addressed before one can definitely understand the structure−property relationships in nanosized rubber-toughened polymers. Research to address the above influences is currently underway and will be reported in the near future.

5. Conclusion

A PEP−PEO diblock copolymer at 5 wt % loading was utilized to toughen bisphenol A type of epoxy. The BCP self-assembled into ca. 15 nm spherical micelles that were well dispersed in the matrix. Mechanical characterization indicates that the PEP−PEO diblock block copolymer can greatly improve the fracture toughness of epoxy without compromising its modulus. The DN-4PB test and TEM observation suggest that the major toughening mechanisms in BCP-toughened epoxy include copolymer micelle cavitation followed by matrix shear banding. The fundamental cause(s) for such a small-scale cavitation process is yet to be determined. The likely contributing factors for the observed nanoscale cavitation phenomenon may include the unique BCP micelle structural characteristics and a possible influence of the surrounding epoxy network, which is significantly modified by the PEO block. Additional research is underway to address the above possibilities.

Acknowledgment. This research was funded by the Dow Chemical Company. J.L. and H.J.S. acknowledge the Microscopy and Imaging Center at Texas A&M University for providing the TEM facilities. Financial support from the Department of Energy through a subcontract to UT-Battelle (No. 4000041622) is gratefully acknowledged by Z.J.T. and F.S.B.

References and Notes

(1) Bucknall, C. B. *Toughened Plastics*; Applied Science: London, 1977.
(2) Kinloch, A. J.; Young, J. *Fracture Behavior of Polymers*; Applied Science: London, 1983.
(3) Kinloch, A. J. In *Toughened Plastics*; Riew, C. K., Ed.; *Adv. Chem. Ser.* **1989**, *67*, 222.
(4) Yee, A. F.; Pearson, R. A. *J. Mater. Sci.* **1986**, *21*, 2462.
(5) Pearson, R. A.; Yee, A. F. *J. Mater. Sci.* **1986**, *21*, 2475.
(6) Pearson, R. A.; Yee, A. F. *J. Mater. Sci.* **1989**, *24*, 2571.
(7) Pearson, R. A.; Yee, A. F. *J. Mater. Sci.* **1991**, *26*, 3828.
(8) Sue, H.-J. *Polym. Eng. Sci.* **1991**, *31*, 275.
(9) Bascom, W. D.; Cottington, R. L.; Jones, R. L.; Peyser, P. *J. Appl. Polym. Sci.* **1975**, *19*, 2545.
(10) Sultan, J. N.; McGarry, F. J. *J. Polym. Eng. Sci.* **1973**, *13*, 29.
(11) Huang, Y.; Kinloch, A. J. *Polymer* **1992**, *33*, 5338.
(12) Sue, H.-J. *J. Mater. Sci.* **1992**, *27*, 3098.
(13) Sue, H.-J.; Garcia-Meitin, E. I.; Orchard, N. A. *J. Polym. Sci., Part B: Polym. Phys.* **1993**, *31*, 595.
(14) Sue, H.-J.; Garcia-Meitin, E. I.; Pickelman, D. M. In *Elastomer Technology Handbook*; Cheremisinoff, N. P., Ed.; CRC Press: Boca Raton, FL, 1993.
(15) Sue, H.-J.; Garcia-Meitin, E. I.; Pickelman, D. M.; Yang, P. C. In *Toughened Plastics*; Riew, C. K., Ed.; *Adv. Chem. Ser.* **1993**, *252*, 161.
(16) Sue, H.-J.; Puckett, P. M.; Garcia-Meitin, E. I.; Bertram, J. L. *J. Polym. Sci., Part B: Polym. Phys.* **1995**, *33*, 2003.
(17) Sue, H.-J.; Yee, A. F. *Polym. Eng. Sci.* **1996**, *36*, 2320.
(18) Sue, H.-J.; Puckett, P. M.; Bertram, J. L.; Walker, L. L.; Garcia-Meitin, E. I. *J. Polym. Sci., Part B: Polym. Phys.* **1999**, *37*, 2137.
(19) Gam, K. T.; Miyamoto, M.; Nishimura, R.; Sue, H.-J. *Polym. Eng. Sci.* **2003**, *43*, 1635.
(20) Borggreve, R. J. M.; Gaymans, R. J.; Eichenwald, H. M. *Polymer* **1989**, *30*, 78.
(21) Borggreve, R. J. M.; Gaymans, R. J.; Schuijer, J. *Polymer* **1989**, *30*, 71.
(22) Borggreve, R. J. M.; Gaymans, R. J.; Schuijer, J.; Ingen Housz, J. F. *Polymer* **1987**, *28*, 1489.
(23) Wu, S. *J. Appl. Polym. Sci.* **1998**, *35*, 549.
(24) Parker, D. S.; Sue, H.-J.; Huang, J.; Yee, A. F. *Polymer* **1990**, *31*, 2267.
(25) Yee, A. F. *J. Mater. Sci.* **1977**, *12*, 757.
(26) Chang, F. C.; Wu, J. S.; Chu, L. H. *J. Appl. Polym. Sci.* **1992**, *44*, 491.
(27) Bubeck, R. A.; Buckley, D. J.; Kramer, E. J.; Brown, H. R. *J. Mater. Sci.* **1991**, *26*, 6249.
(28) Breuer, H.; Haaf, F.; Stabenow, J. *J. Macromol. Sci. Phys.* **1977**, *14*, 387.
(29) Haaf, F.; Breuer, H.; Echte, A.; Schmitt, B. J.; Stabenow, J. *J. Sci. Ind. Res.* **1981**, *40*, 659.
(30) Tse, A.; Shin, E.; Hiltner, A.; Baer, E.; Laakso, R. *J. Mater. Sci.* **1991**, *26*, 2823.
(31) Hourston, D. J.; Lane, S.; Zhang, H. X. *Polymer* **1991**, *32*, 2215.
(32) Azimi, H. R.; Pearson, R. A.; Hertzberg, R. *J. Mater. Sci.* **1996**, *31*, 3777.
(33) Lazzeri, A.; Bucknall, C. B. *J. Mater. Sci.* **1993**, *28*, 6799.
(34) Bucknall, C. B.; Karpodinis, A.; Zhang, X. C. *J. Mater. Sci.* **1994**, *29*, 3377.
(35) Lazzeri, A.; Bucknall, C. B. *Polymer* **1995**, *26*, 2895.
(36) Gaymans, R. J.; Borggreve, R. J. M.; Oostenbrink, A. J. *Makromol. Chem., Macromol. Symp.* **1990**, *38*, 125.
(37) Kim, D. S.; Cho, K.; Kim, J. K.; Park, C. E. *Polym. Eng. Sci.* **1996**, *36*, 755.
(38) Bates, F. S.; Berney, C. V.; Cohen, R. E. *Macromolecules* **1983**, *16*, 1101.
(39) Bates, F. S.; Cohen, R. E.; Argon, A. S. *Macromolecules* **1983**, *16*, 1108.
(40) Schwier, C. E.; Argon, A. S.; Cohen, R. E. *Philos. Mag. A* **1985**, *52*, 581.
(41) Hillmyer, M. A.; Lipic, P. M.; Hajduk, D.; Almdal, K.; Bates, F. S. *J. Am. Chem. Soc.* **1997**, *119*, 2749.
(42) Lipic, P. M.; Bates, F. S.; Hillmyer, M. A. *J. Am. Chem. Soc.* **1998**, *120*, 8963.
(43) Grubbs, R. B.; Broz, M. E.; Dean, J. M.; Bates, F. S. *Macromolecules* **2000**, *33*, 2308.
(44) Grubbs, R. B.; Broz, M. E.; Dean, J. M.; Bates, F. S. *Macromolecules* **2000**, *33*, 9522.
(45) Dean, J. M.; Lipic, P. M.; Grubbs, R. B.; Cook, R. F.; Bates, F. S. *J. Polym. Sci., Part B: Polym. Phys.* **2001**, *39*, 2996.
(46) Grubbs, R. B.; Dean, J. M.; Bates, F. S. *Macromolecules* **2001**, *34*, 8593.
(47) Dean, J. M.; Grubbs, R. B.; Saad, W.; Cook, R. F.; Bates, F. S. *J. Polym. Sci., Part B: Polym. Phys.* **2003**, *41*, 2444.
(48) Dean, J. M.; Verghese, N. E.; Pham, H. Q.; Bates, F. S. *Macromolecules* **2003**, *36*, 9267.
(49) Guo, Q.; Dean, J. M.; Grubbs, R. B.; Bates, F. S. *J. Polym. Sci., Part B: Polym. Phys.* **2003**, *41*, 1994.
(50) Sumeet, J.; Bates, F. S. *Science* **2003**, *300*, 460.
(51) Wu, J.; Thio, Y. S.; Bates, F. S. *J. Polym. Sci., Part B: Polym. Phys.* **2005**, *43*, 1950.
(52) Girard-Reydet, E.; Pascault, J. P.; Bonnet, A.; Court, F.; Leibler, L. *Macromol. Symp.* **2003**, *198*, 309.
(53) Hydro, R. M.; Pearson, R. A. *J. Polym. Sci., Part B: Polym. Phys.* **2007**, *45*, 1470.
(54) Hillmyer, M. A.; Bates, F. S. *Macromolecules* **1996**, *29*, 6994.
(55) Lesser, A. J.; Crawford, E. *J. Appl. Polym. Sci.* **1997**, *66*, 387.
(56) Neilsen, L. E. *J. Macromol. Sci.* **1969**, *C3*, 69.
(57) Neilsen, L. E.; Landel, R. F. *Mechanical Properties of Polymers and Composites*, 2nd ed.; Marcel Dekker: New York, 1994.
(58) Sue, H.-J.; Pearson, R. A.; Parker, D. S.; Huang, J.; Yee, A. F. *Polym. Prepr.* **1988**, *29*, 147.
(59) Sue, H.-J. *Polym. Eng. Sci.* **1991**, *31*, 270.
(60) Sue, H.-J.; Yee, A. F. *J. Mater. Sci.* **1993**, *28*, 2975.
(61) Holik, A. S.; Kambour, R. P.; Hobbs, S. Y.; Fink, D. G. *Microstruct. Sci.* **1979**, *7*, 357.
(62) Liu, J.; Sue, H.-J.; Thompson, Z. J.; Bates, F. S.; Dettloff, M.; Jacob, G.; Verghese, N.; Pham, H. To be submitted.
(63) Sue, H.-J.; Yang, P. C.; Garcia-Meitin, E. I.; Bishop, M. T. *J. Mater. Sci. Lett.* **1993**, *12*, 1463.
(64) Kinloch, A. J.; Williams, J. G. *J. Mater. Sci.* **1980**, *15*, 987.
(65) Dompas, D.; Groeninckx, G. *Polymer* **1994**, *35*, 4743.
(66) Fond, C.; Lobbrecht, A.; Schirrer, R. *Int. J. Fract.* **1996**, *77*, 141.
(67) Smit, R. J. M.; Brekelmans, W. A. M.; Meijer, H. E. H. *J. Mater. Sci.* **2000**, *35*, 2869.
(68) Bucknall, C. B. In *The Physics of Glassy Polymers*, 2nd ed.; Haward, R. N., Young, R. J., Eds.; Chapman & Hall: London, 1997; p 363.
(69) Hasan, O. A.; Boyce, M. C.; Berko, S. *J. Polym. Sci., Part B: Polym. Phys.* **1993**, *31*, 185.
(70) Hristov, H. A.; Bolan, B.; Yee, A. F.; Xie, L.; Gidley, D. W. *Macromolecules* **1996**, *29*, 8507.
(71) Bartos, J.; Bandzuch, P.; Sausa, O.; Kristiakova, K.; Kristiakova, J.; Kanaka, T.; Jenninger, W. *Macromolecules* **1997**, *30*, 6906.
(72) Bucknall, C. B. *J. Polym. Sci., Part B: Polym. Phys.* **2007**, *45*, 1399.
(73) Gent, A. N. *J. Polym. Sci. Symp.* **1974**, *48*, 1.
(74) Harper, C. A. *Handbook of Plastics and Elastomers*; McGraw-Hill Book Co.: New York, 1975.
(75) Jho, J. Y.; Yee, A. F. *Macromolecules* **1991**, *24*, 1905.
(76) Xiao, C.; Jho, J. Y.; Yee, A. F. *Macromolecules* **1994**, *27*, 2761.
(77) Lee, P. L.; Kowalewski, T.; Poliks, M. D.; Schaefer, J. *Macromolecules* **1995**, *28*, 2476.
(78) Menard, K. P., *Dynamic Mechanical Analysis: A Practical Introduction*; CRC Press: Boca Raton, FL, 1999.
(79) Wendorf, J. H.; Fischer, E. W. *Kolloid Z. Z. Polym.* **1973**, *251*, 876.
(80) David, L.; Vigier, G.; Etienne, S.; Faivre, A.; Soles, C.; Yee, A. F. *J. Non-Cryst. Solids* **1998**, *235*−*237*, 383.
(81) Yang, L.; Hristov, H. A.; Yee, A. F.; Gidley, D. W.; Bauchiere, D.; Halary, J. L.; Monnerie, L. *Polymer* **1995**, *36*, 3997.

MA801037Q